

# Real-Time Protein Binding Detection with Neuromorphic Integrated Sensor

Blake C. Jacquot\*, N. L. Muñoz\*, D. W. Branch<sup>†</sup>, E. C. Kan\*

\*School of Electrical and Computer Engineering, Cornell University, Ithaca, NY 14853, bcj7@cornell.edu

<sup>†</sup>Sandia National Laboratories, Albuquerque, NM 87185

**Abstract**—Real time protein binding interactions between biotinylated bovine serum albumen (BSA) and streptavidin (SA) are detected using chemoreceptive neuron MOS (CvMOS) transistors with extended floating gate structures. This enables protein interaction events to be monitored by a sensing gate area that is only capacitively coupled to the sensing circuits and far removed from the active area, reducing the invasiveness without loss of sensitivity. The use of both sensing and control gates to control the floating gate potential eliminates the need of an analyte reference electrode.

**Index Terms**—Protein microarray, biosensor, FET, floating-gate, chemical sensor

## I. INTRODUCTION

Silicon-based field-effect devices benefit from many advantages that make them ideal candidates for electrochemical sensors in biological applications. These include reduced size and weight, fast response, large bandwidth, high reliability, low-power consumption, and ready integration with standard CMOS processes. The latter makes it possible to have on-chip integration of sensor arrays with signal processing schemes for low-cost mass production in comparison to the other existing technologies such as mass spectroscopy, optical measurements and faradaic electrochemical measurements [1-6].

Unlike other field effect transistor (FET)-based sensors (e.g. ISFET, ENFET, GASFET, CHEMET) [7], the chemoreceptive neuron metal-oxide-silicon (CvMOS) device uses an extended floating gate structure to allow the sensing area to be far removed from the active area [8, 9]. This separation reduces the likelihood of impairing the underlying FET with the application of fluids containing alkali ions. The sensing area, or sensing gate (SG), couples to the extended floating gate capacitively and dominates device response due to its large size in comparison to the other structures of FET. Multiple sensing gates can be coupled to the extended floating gate, analogous to multiple dendrite inputs to a neuron cell, hence the name CvMOS [9-11]. The control gate (CG) is AC or DC biased and also provides a capacitively coupled input to the extended floating gate, which, in turn interacts with the underlying FET. The ability to regulate the floating gate potential with both sensing and control gates permits the recognition of protein binding events through impedance changes without

the need of massive analyte reference electrodes and allows for the device to be held in saturation during measurement. The large-signal drain current  $I_d$  of the FET is a function of the floating gate potential:

$$I_d = \frac{\kappa_n}{2} (V_{fg} - V_t)^2 \quad (1)$$

where  $\kappa_n$  is the transconductance parameter ( $A/V^2$ ),  $V_t$  is the threshold voltage and  $V_{fg}$  is the floating gate potential.

This paper presents the experimental results of the first neuron FET-based [10] sensing using a single frequency stimulus at the control gate for real-time monitoring of protein binding in fluid. A biotinylated-BSA-SA was chosen because of its well-known properties to demonstrate the dynamic sensing capabilities of CvMOS. The successful detection of BSA-SA binding interactions with demonstrated resolution of to  $0.025\mu\text{g}/\text{cm}^2$  makes CvMOS a strong contender for biosensing applications. Other protein systems, such as IgG, have been measured but are not presented here.

## II. DEVICE DESIGN AND FABRICATION

The CvMOS device architecture resembles that of a Flash memory cell (Fig. 1) [12]. The control and sensing gates independently couple to the floating gate, which in turn sets the underlying FET channel potential that controls the drain current output according to Eq. (1). The CvMOS devices in this study were fabricated via the MOSIS foundry service using the AMIS 1.5  $\mu\text{m}$  process [13]. Tests were carried out on devices that had one single sensing gate with sensor areas ranging from  $23\mu\text{m} \times 360\mu\text{m}$  to  $157\mu\text{m} \times 360\mu\text{m}$

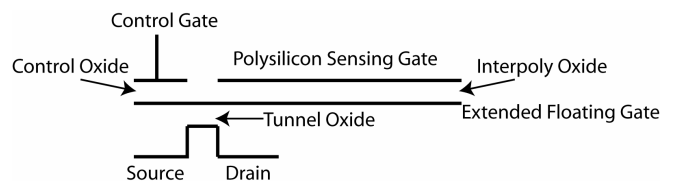


**Fig. 1:** Schematics of a CvMOS transistor. The MOS area is similar to the commercial Flash memory cell in structure and fabrication process.

### III. EXPERIMENTS

Prior to experiments, the CvMOS devices and witness samples were thoroughly rinsed with acetone, methanol, isopropanol and de-ionized water for organic removal, and were exposed to a UV/ozone cleaning system (Bioforce Nanoscience) for 15 minutes. A silane monolayer was immobilized on the SiO<sub>2</sub> surface by placing the samples in a mixture of (3-glycidioxypropyl)trimethylethoxysilane (3-GPS) in toluene for 1 hr, followed by a 1-hr bake at 120°C to complete the covalent linkage. Biotinylated-BSA was then covalently bound to the 3-GPS monolayer by exposure for 2 hours and the surface was then rinsed with 1X phosphate-buffered saline (PBS) to remove non-bound proteins, and then DI water to remove excess salt.

A function generator (Stanford Reseach DS345) was used to deliver a 10Vpp, 20kHz AC voltage to the control gate and the reference input of a lock-in amplifier (Stanford Research 380) (Fig. 2). The CvMOS architecture allows this AC signal to be coupled to both the extended floating gate to create the inversion channel in the FET and to the sensing interface where binding events are taking place. The drain and source were biased at 5V and 0V respectively. The output drain current was transduced to a voltage via a transimpedance amplifier (Stanford Research SR570) and fed to both the lock-in amplifier at 100μA/V and an oscilloscope (Tektronix TDS 340A) to monitor the expected waveform output. The data was analyzed from the lock-in as the RMS voltage over time.

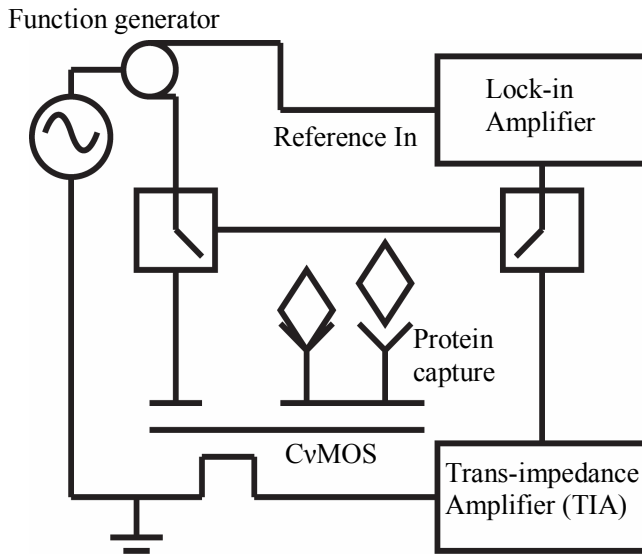


Fig. 2: The block diagram of measurement circuits with CvMOS as the protein sensor.

Fluids were directly delivered to the sensing gate with a micro-pipette. The sensing gate areas were isolated from the electrical contact pads via a polymethylsiloxane (PDMS) chamber.

The sensor readout was allowed to stabilize with 40μL of 0.1X PBS with 20% glycerol prior to adding the streptavidin (SA) target analyte. The glycerol helped to lessen noise from any convective fluid flow. Witness samples underwent the same treatment, minus the glycerol. 10μL of 0.02mg/mL SA 0.1X PBS was then added to the sensor and witness samples. The sensor drain current response in the specific excitation frequency was monitored in real time.

Protein layer thickness was measured on the witness samples with an imaging ellipsometer (Nanofilm Surface Analysis) at a 632 nm wavelength. The total surface coverage of the silane and protein layers may be expressed as a function of the refractive index, bulk density and sample thickness. By taking an estimate of the cross-sectional area of both the organosilane and SA molecule, the percentage surface coverage can be calculated.

### IV. SENSORS MODELS

An impedance model is used to approximate the interaction of the functionalized sensing gate surface with analyte in a fluidic environment (Fig. 3). Because the resistive component is negligible when sensing across high-resistance oxides, each protein layer is modeled as a capacitive element stacked over the SG with its respective capacitance given by:

$$C = \frac{\epsilon_o \epsilon_r A}{d} \quad (2)$$

where  $\epsilon_o$  is vacuum permittivity,  $\epsilon_r$  is the dielectric constant,  $A$  is the sensor surface area and  $d$  is sample thickness.  $\epsilon_r$  was 4.5, 11.8, 10, and  $\geq 78$  for SiO<sub>2</sub>, 3-GPS, protein, and water, respectively.

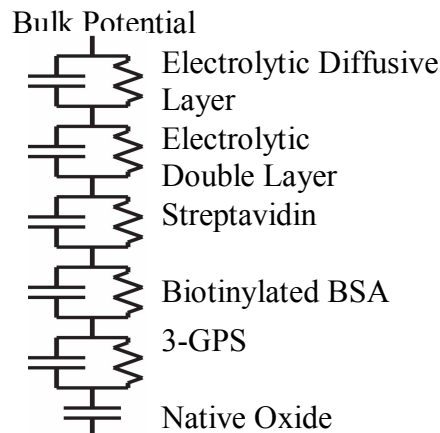


Fig. 3: Impedance model of the sensing interface. 3-GPS creates covalent bond with BSA. Streptavidin acts as the analyte. Total capacitance decreases as analyte thickness increases.

A Gouy-Chapman Stern (CGS) model is used to describe the fluid interface, with  $C_{EDL}$  and  $C_{diff}$  being the double-layer and diffusive capacitances, respectively [14]. These capacitive layers are large relative to the protein layer capacitances and can be neglected without significant

inaccuracy. Thicknesses for the double layer and diffusive layer are assumed as 5 Å and 25 Å respectively. With these capacitances known, as well as  $C_b$  and  $C_{cg}$ , the parasitic bulk capacitance and control gate capacitance, the total floating gate capacitance and potential may be expressed as:

$$C_T \cong C_b + C_{cg} + C_{sg} \parallel C_{ox} \parallel C_{3-GPS} \parallel C_{BSA} \parallel C_{strep} \parallel C_{EDL} \parallel C_{diff} \quad (3).$$

$$V_{fg} \cong \frac{Q + V_{cg} C_{cg}}{C_T} \quad (4)$$

Here,  $C_T$  is total capacitance of floating gate,  $C_{sg}$  is the interpoly oxide capacitance at the sensing gate,  $C_{ox}$  is the native oxide capacitance at the sensing gate,  $C_{3-GPS}$  is the capacitance of the 3-GPS layer, and  $C_{BSA}$  and  $C_{strep}$  are the protein layer capacitances.  $V_{fg}$  is the voltage of the floating gate,  $Q$  is the static charge in the floating gate, and  $V_{cg}$  is the voltage applied at the control gate.

With  $k_n$  and  $V_i$  known from the foundry technology file, Eq. (1) can be expressed as a variable of  $V_{fg}$  in Eq. (4) which depends on  $Q$ , a parameter that was held constant after model calibration. A large-signal RMS floating gate potential can thus be extracted and plotted against captured protein thickness (Fig. 4).

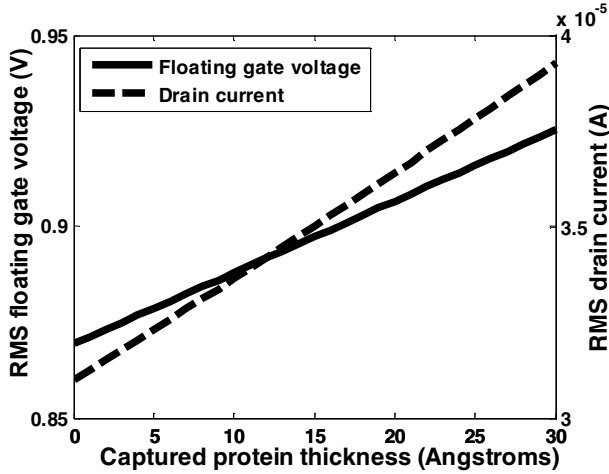


Fig. 4: Expected RMS voltage change on floating gate for variation in protein thickness according to the CvMOS model.

## V. RESULTS/DISCUSSION

The real-time RMS response to biotinylated-BSA-SA binding events reveals that sensor signal increases upon addition of the SA analyte as predicted by the model (Fig. 5). The capture event corresponds to an analyte thickness change of 18.6 Å, which is equivalent to about 69% surface coverage. The signal saturates as available surface sites become occupied. The control test shows no net variation upon addition of a control test of a PBS drop of same size.

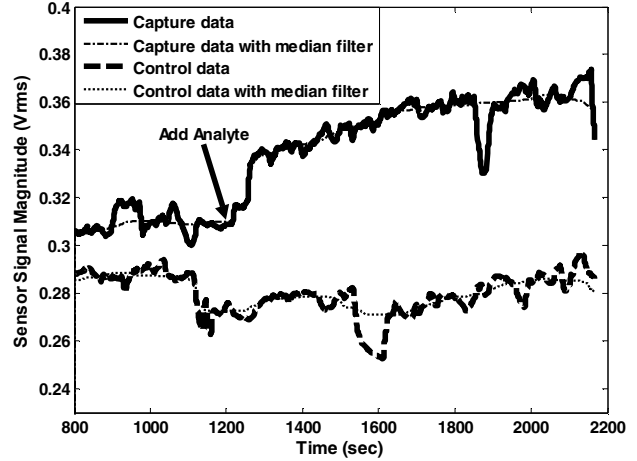


Fig. 5: Real-time detection of roughly 18.6 Å (or roughly 69% surface coverage) of streptavidin binding to biotinylated-BSA and control test in electrolytic fluid at 20kHz. Ionic fluid creates substantial noise.

A calibration curve such as the one of Fig. 6 may be extracted from the response of the CvMOS sensor and ellipsometry, as compared to control experiments where only PBS was added. SA thickness was measured to range from 3 Å to 18.6 Å, with equivalent captured mass ranging from 0.04 μg/cm<sup>2</sup> to roughly 0.25 μg/cm<sup>2</sup> (Fig. 6). Also, the measured protein layer thickness values from the RMS floating gate potential, as extracted from Eqs. (3) and (4) may be plotted against those measured on the witness samples with the ellipsometer (Fig. 7). Surface coverage was found to range from 11% to 69%.

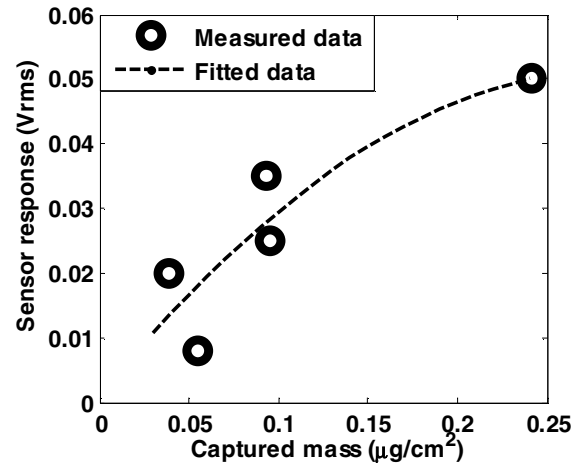


Fig. 6: The calibration curve constructed from 20 kHz sensor monitoring over several samples. Plot shows actual amount bound and not amount to which the sensor was exposed. Sensor measurements conform to the device model in Eqs. (3) and (4). Protein thickness measured by ellipsometer from witness samples can be used in conversion of surface coverage or captured mass.

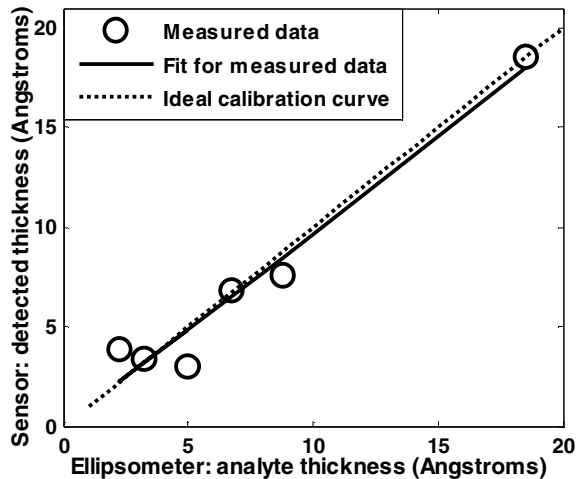


Fig. 7: Detected thickness extracted from large-signal sensor model versus analyte thickness measured by ellipsometer on witness samples. Protein thickness measured by ellipsometer can be converted to surface coverage, here ranging from 11% to 69%.

Figure 7 reveals that the CvMOS sensor is capable of detecting down to a 2 Å change in the SA layer thickness. This corresponds to approximately a  $0.025\mu\text{g}/\text{cm}^2$  resolution on the order of 50s. Figure 6 shows sensor response begins to saturate at around an estimated value of 69% surface coverage, equivalent to  $0.25\mu\text{g}/\text{cm}^2$ .

## VI. CONCLUSIONS

CvMOS is shown to successfully detect the protein binding events between BSA and SA on the order of  $0.025\mu\text{g}/\text{cm}^2$  or 2 Å thickness through monitoring at a single AC frequency. A model of the sensor and the sensor interface were determined and verified experimentally. This capacitive sensing approach is found to eliminate the need for a reference potential in the analyte, thus reducing the invasiveness, size and weight of the sensor, all which are desired criteria for field-deployable sensor technologies.

## ACKNOWLEDGMENT

This project is supported by the Environmental Protection Agency (EPA), Sandia National Laboratories and NYSTAR.

## REFERENCES

- [1] D.S. Kim, H.J. Park, H.M. Jung, J.K. Shin, P. Choi, J.H. Lee, and G. Lim, "FET-based biomolecular sensors employing Pt reference electrode for the detection of DNA sequence," *Japanese Journal of Applied Physics*, vol. 43, no. 6B, pp. 3855-3859, 2004.
- [2] E. Bakker, "Electrochemical sensors," *Anal. Chem.*, vol. 76, pp. 3285-3298, 2004.
- [3] D.M. Wilson, S. Hoyt, J. Janata, K. Booksh and L. Obando, "Chemical Sensors for Portable, Handheld Field Instruments," *IEEE Sensors Journal*, vol. 1, pp. 256-274, 2001.
- [4] E. Katz and I. Willner, "Probing biomolecular interactions at conductive and semiconductive surfaces by impedance spectroscopy" *Electroanalysis*, vol. 15, pp. 913-947, 2003.

- [5] M. Zhang, M. R. Haider, M. A. Huque, M. A. Adeb, S. Rahman, and S. K. Islam, *Smart Materials and Structures*, vol. 16, pp. 525-530, 2007.
- [6] N.F. Chiu, J.M. Wang, C.W. Liao, C.H. Chen, H.C. Chen, L.J. Yang, S.S. Lu, C.W. Lin, "An Implantable Multifunctional Needle Type Biosensor with Integrated RF Capability," in *Eng. Med. Biol. Soc., Proceedings of IEEE*, 2005, pp. 1933-1936.
- [7] P. Bergveld, "Thirty years of ISFETOLOGY" *Sensors and Actuators, B: Chemical*, vol. 88, pp. 1-20, 2003.
- [8] B. C. Jacquot, C. Lee, Y. N. Shen and E. C. Kan, "Time-resolved ion and molecule transport sensing with microfluidic integration by chemoreceptive neuron MOS transistors (CvMOS)," in *Sensors, Proceedings of IEEE*, 2005, pp. 101-104.
- [9] N. Y. Shen, Z. Liu, C. Lee, B. A. Minch and E. C. Kan, "Charge-based chemical sensors: a neuromorphic approach with chemoreceptive neuron MOS (CvMOS) transistors," *Electron Devices, IEEE Transactions on*, vol. 50, pp. 2171-2178, 2003.
- [10] T. Shibata and T. Ohmi, "A functional MOS transistor featuring gate-level weighted sum and threshold operations," *Electron Devices, IEEE Transactions on*, vol. 39, pp. 1444-1455, 1992.
- [11] B. A. Minch, C. Diorio, P. Hasler, and C. A. Mead, "Translinear circuits using subthreshold floating-gate MOS transistors," *Analog Integrated Circuits and Signal Processing*, vol. 9, no. 2, pp. 167-179, 1996.
- [12] J.M. Rabaey, A. Chandrakasan and B. Nikolic, *Digital Integrated Circuits*, Upper Saddle River, NJ: Prentice Hall, 2003.
- [13] "<http://www.mosis.org/Technical/Processes/proc-ami-abn.html>."
- [14] A.J. Bard and L.R. Faulkner, *Electrochemical Methods: Fundamentals and Applications*, New York, NY: Wiley, 2000.